Original Paper

Eletrônica de Potência
Open Journal of Power Electronics

Received March 17, 2024; accepted June 13, 2024; Date of publication July 04, 2024.
The review of this paper was arranged by Associate Editor Fernanda M. Carnielutti and Editor-in-Chief Heverton A. Pereira

Digital Object Identifier http://doi.org/10.18618/REP.2005.1.045052

Large-Signal Models of the Park Transformation and Phase-Locked Loop Algorithms

Edhuardo F. C. Grabovski[1], Samir A. Mussa[1], Marcelo L. Heldwein[2]

[1]Federal University of Santa Catarina, Power Electronics Institute, Florianópolis – SC, Brazil.
[2]Technical University of Munich, Chair of High-Power Converter Systems, Munich, Germany.

e-mail: edhuardo.celli@gmail.com; samir@inep.ufsc.br; marcelo.heldwein@tum.de.

ABSTRACT The control of modern grid-connected converters often relies on Park Transform and synchronization algorithms. These are highly nonlinear subsystems integrated into even larger systems that include other nonlinearities. Thus, strictly speaking, large-signal models are required when analysing and designing such systems. However, a limited number of mathematical tools is available to that end. This work proposes a nonlinear time-invariant model for the Park Transformation and the Synchronous Reference Frame Phase-Locked Loop (SRF-PLL), which are based on the Harmonic State-Space (HSS) in a stationary coordinate frame. The HSS modeling technique is reviewed as a basis for nonlinear models of functions based on polynomial nonlinear systems. This serves as an appropriate formal basis for the model of 2-D rotations as means of modeling the SRF-PLL and other similar algorithms. The models are validated through simulations to verify their accuracy when compared to the original Nonlinear Time-Periodic (NLTP) Systems.

KEYWORDS ac power electronic systems, control oriented models, dynamic phasor modeling, harmonic state-space modeling, large-signal modeling, time-periodic systems.

I. INTRODUCTION

The ever increasing demand for power converters to interface different energy resources with an electric grid paved the way for the insertion of distributed energy resources and energy-saving applications, while guaranteeing an appropriate operation for a wide range of conditions. Over the last few decades, the state-of-the-art evolved in a way dictated by those trends, with a special focus on the reliability of renewable power systems, which is dependent on the system stability and power quality ensured by the control strategies [1]–[3].

The more commonly employed control strategies can be separated into multiple-timescale control system as means of regulating the electrical quantities as means of guaranteeing an adequate system behaviour [3]–[5]. These control dynamics can involve electromechanical dynamics and electromagnetic transients of power networks, which may lead to instabilities and/or oscillations, especially when the system has an increased penetration of power converters [6], [7].

In the recent years, there has been an increase in demand for more faithful mathematical models representing such effects, which typically discard the eventual presence of harmonics [8] or take advantage of multiple-frequency averaging models [9] and Dynamic Phasor (DP) or Harmonic State-Space (HSS) approaches [10]–[12]. These approaches aim to perform and analyze the projection of the infinite-dimensional characteristic of Nonlinear Time-Periodic (NLTP) systems, which are described relating to state and input/disturbance variables expressed in terms of $L^2(\mathcal{P})$ functions with respect to a certain set $\mathcal{P}$, into a finite dimensional time-invariant space which can be complex- or real-valued depending on the adopted approach.

Furthermore, the state-of-the-art analysis are usually performed over small-signal dynamics [13]–[16], which hinders the identification of limit-cycles and the presence of multiple equilibrium points or a possible chaotic behaviour which can be caused by the inherent nonlinear characteristic of the control loops while significantly reducing the complexity of the mathematical models. Concerns can also be raised over the validity of small-signal models, especially under weak-grid conditions, which present a higher degree of cross-coupling between control loops.

An accurate description of the control loops is dependent on the dynamics of the synchronism loops when considering grid-following systems. A commonly adopted approach is to employ linearized models of Phase-Locked Loops (PLLs) due to the complexity of the trigonometric functions and their description in the harmonic domain. The validity of the use of linearization is here again of concern.

Therefore, the contributions aimed by this article are to demonstrate the model of nonlinear mathematical function models in the infinite-dimensional harmonic domain, which can be truncated for a finite number of harmonics. Hence, a detailed mathematical analysis of such tool is presented in a first moment as means of providing a framework for the expansion of the use of HSS modeling technique, as the

current state-of-the-art mainly focuses on linear analysis, by applying linearizations to models before calculating a point of equilibrium, which can lead to subsequent modeling errors and inaccurate further analysis.

These validated models are then employed with the objective of modeling 2-D vector rotations and the division between two real-valued functions as means of obtaining a Nonlinear Time-Invariant (NLTI) model of the Park-Transformation and the Synchronous-Reference Frame Phase-Locked Loop (SRF-PLL), which serves as a base for more complex synchronism strategies [17]–[19]. Thus, each step is thoroughly validated as means of demonstrating the effect of truncations on each modeling step, as the final model contains a large degree-of-freedom, and these steps should provide a guideline on the number of terms and number of harmonics required for an accurate description of the subsequent model.

The use of the modeling strategies here proposed can also be employed for different applications, as the creation of a framework is initially intended, and then expanded for specific applications, in this case a SRF-PLL which consider multiple harmonics. Note that even though the validations shown here in the time-variant domain through the recreation of the time-variant signals, the resulting models are NLTI, which enables an accurate calculation of the points of equilibrium, and subsequent stability analysis of system can be performed following the presented methodology.

In a first moment, an overview of the Harmonic State-Space models for linear systems and nonlinear polynomial systems is presented, which serves as a base for the exponential function model and the division of two signals employed in the normalisation. The subsequent section demonstrates the 2-D rotation of a vector employed in the Park Transformation with the objective of modeling the rotation angle in the HSS. Lastly, a NLTI model of the SRF-PLL model is expressed with its subsequent validation. Experimental results employing hardware-in-the-loop simulation of a grid-connected Voltage Source Inverter with control strategy implemented in an FPGA-Microprocessor and are also shown as means of validating the discussed models.

II. HARMONIC STATE-SPACE OVERVIEW

The present analysis is divided into a recapitulation of the HSS and DP modeling, and their application related to more complex state-space models of nonlinear functions, as means of obtaining nonlinear models in reference of certain desired inputs and outputs.

A. A REVIEW OF LINEAR TIME-VARIANT SYSTEMS

Let a linear state-space model of a certain dynamic system be described by

$$D_t\mathbf{x} = \mathbf{A}\mathbf{x} + \mathbf{B}\mathbf{u}, \tag{1}$$

where D_t is the derivative operator with respect to t, $\mathbf{A} \in \mathbb{R}^{n_x \times n_x}$, $\mathbf{B} \in \mathbb{R}^{n_x \times n_u}$, $\mathbf{x} \in \mathcal{X} \subseteq L^2(\mathbb{R}^{n_x})$ and $\mathbf{u} \in \mathcal{U} \subseteq L^2(\mathbb{R}^{n_u})$, in a manner that

$$\begin{aligned} x_i(t) &:= \sum_{k=-\infty}^{\infty} x_{i,k}(t) = \sum_{k=-\infty}^{\infty} \langle x_i(t)\rangle_k e^{\iota k\theta(t)} \\ u_i(t) &:= \sum_{k=-\infty}^{\infty} u_{i,k}(t) = \sum_{k=-\infty}^{\infty} \langle u_i(t)\rangle_k e^{\iota k\theta(t)}, \end{aligned} \tag{2}$$

$\forall i \in \mathbb{Z}^{n_x}$, where $\langle x\rangle_k$ is the k^{th} harmonic dynamic phasor for an arbitrary angle

$$\theta := \theta_0 + \int_{-\infty}^{t} \omega(\tau)\mathrm{d}\tau \tag{3}$$

and $\iota^2 := -1$. Each dynamic phasor can be interpreted as the projection of the initial of a signal onto the exponential function $e^{\iota k\theta}, \forall k \in \mathbf{Z}$, which can be interpreted as the coefficients of the Fourier Transform.

Thus, the HSS model of (1) can be written in accordance with

$$\begin{aligned} D_t \langle\mathbf{x}\rangle &= (\mathbf{I}_\infty \otimes \mathbf{A} - \mathbf{G}) \langle\mathbf{x}\rangle + (\mathbf{I}_\infty \otimes \mathbf{B}) \langle\mathbf{u}\rangle \\ \mathbf{G} &:= \operatorname{diag}(\mathbb{Z}) \otimes \iota\omega\mathbf{I}_{n_x}, \end{aligned} \tag{4}$$

where $\left\{\langle\mathbf{x}\rangle \in \ell^2(\mathbb{C}^{n_x}) : \langle\mathbf{x}\rangle = (\langle\mathbf{x}\rangle_k)_{-\infty}^{\infty}\right\}$ is the set of dynamic phasors of $\mathbf{x}$ and $\otimes$ is the tensor product. The HSS model can be truncated for a finite number of harmonics $n_h < \aleph_0$, assuming that the system has a low-pass characteristic when $\omega \to \infty$, as the characteristic polynomial of the HSS system, which is given by

$$\begin{aligned} p(\lambda) &= \det\left(\lambda\mathbf{I} - (\mathbf{I}_\infty \otimes \mathbf{A} - \mathbf{G})\right) \\ &= \prod_{k=-\infty}^{\infty} \det\left((\lambda - \iota k\omega)\mathbf{I} - \mathbf{A}\right), \end{aligned} \tag{5}$$

as $\lambda_k \to \iota k\omega$ for larger values of $|k|$. In this case,

$$\begin{aligned} \operatorname{span}\left(D_t\langle\mathbf{x}\rangle\right) &= \bigoplus_{k=-\infty}^{\infty} \operatorname{span}\left(D_t\langle\mathbf{x}\rangle_k\right) \\ &\approx \bigoplus_{h=-n_h}^{n_h} \operatorname{span}\left(D_t\langle\mathbf{x}\rangle_k\right), \end{aligned} \tag{6}$$

for

$$\mathbf{x} = \sum_{h=-\infty}^{\infty} \langle\mathbf{x}\rangle_h e^{\iota h\omega t + \theta_0} \approx \sum_{h=-n_h}^{n_h} \langle\mathbf{x}\rangle_h e^{\iota h\omega t + \theta_0}, \tag{7}$$

where $\bigoplus$ is the direct sum operator, as each frequency subspace is decoupled, i.e., we can write a separate decoupled system for each harmonic frequency. This is not always true for nonlinear systems, as the frequency components are coupled through the nonlinearities of the systems, as further discussed in the next subsection.

The HSS and DP models are related by the linear map $f : \mathbb{C}^2 \to \mathbb{R}^2$ such that

$$\begin{bmatrix} \Re\{\langle x\rangle_h\} \\ \Im\{\langle x\rangle_h\} \end{bmatrix} = \frac{1}{2}\begin{bmatrix} 1 & 1 \\ -\iota & \iota \end{bmatrix}\begin{bmatrix} \langle x\rangle_h \\ \langle x\rangle_{-h} \end{bmatrix} \tag{8}$$

for a certain harmonic component h. Since $x \in \mathbb{R}$, we have that

$$\langle x\rangle_{-h} = \langle x\rangle_h^*, \tag{9}$$

$$\mathbf{\Gamma} \circ \langle u \rangle = \begin{bmatrix} \langle u \rangle_0 & \langle u \rangle_{-1} & \cdots & \langle u \rangle_{-h} & & & \\ \langle u \rangle_1 & \ddots & \ddots & \ddots & \ddots & & \\ \vdots & \ddots & \langle u \rangle_0 & \langle u \rangle_{-1} & \ddots & \ddots & \\ \langle u \rangle_h & \ddots & \langle u \rangle_1 & \langle u \rangle_0 & \langle u \rangle_{-1} & \ddots & \langle u \rangle_{-h} \\ & \ddots & \ddots & \langle u \rangle_1 & \langle x \rangle_0 & \ddots & \vdots \\ & & \ddots & \ddots & \ddots & \ddots & \langle u \rangle_{-1} \\ & & & \langle u \rangle_h & \cdots & \langle u \rangle_1 & \langle u \rangle_0 \end{bmatrix} \tag{13}$$

which in turn makes f bijective.

From this, we can define a linear map $\mathbf{\Psi} : \ell^2(\mathbb{C}) \to \ell^2(\mathbb{R})$ so that $\left(\Re\left\{\langle x \rangle\right\}, \Im\left\{\langle x \rangle\right\}\right) = \mathbf{\Psi} \circ \langle x \rangle$, where

$$\mathbf{\Psi} = \frac{1}{2} \begin{bmatrix} \mathbf{I} & \mathbf{0} & \mathbf{J} \\ \mathbf{0} & 1 & \mathbf{0} \\ \iota\mathbf{I} & \mathbf{0} & -\iota\mathbf{J} \end{bmatrix} \tag{10}$$

and $\mathbf{J}$ is an exchange (or backward identity) matrix. We can also define a linear map $\mathbf{\Psi}_n : \ell^2(\mathbb{C}^n) \to \ell^2(\mathbb{R}^n)$ as

$$\mathbf{\Psi}_n = \mathbf{\Psi} \otimes \mathbf{I}_n, \tag{11}$$

leading to $\left(\Re\left\{\langle \mathbf{x} \rangle\right\}, \Im\left\{\langle \mathbf{x} \rangle\right\}\right) = \mathbf{\Psi}_{n_x} \circ \langle \mathbf{x} \rangle$.

However, the equations presented in (4) and (6) are not valid for nonlinear systems, since nonlinearities, in general, introduce a coupling between harmonic components, as further discussed.

B. ON THE MODEL OF POLYNOMIAL NONLINEAR SYSTEMS

Let $u, v \in L^2(\mathbb{R})$. From the convolution properties of the Fourier Transform, we can write the multiplication of both signals in the time domain as the convolution in the frequency domain. Since $\langle x_i \rangle \in \ell^2(\mathbb{C}), \ \forall i \in \{1, 2\}$, the operation turns into a discrete convolution given by

$$\langle uv \rangle_h = \sum_{j=-\infty}^{\infty} \langle u \rangle_j \langle v \rangle_{h-j} \tag{12}$$

for each harmonic component $h \in \mathbb{N}$. We can also employ the Toeplitz operator $\mathbf{\Gamma}(\cdot)$ defined by (13) as means of solving (12), resulting in

$$\langle uv \rangle = \left(\mathbf{\Gamma} \circ \langle u \rangle\right) \circ \langle v \rangle. \tag{14}$$

From (14), we can write the dynamic phasor for the powers of a signal as

$$\begin{aligned} \langle u \rangle &= \left(\mathbf{\Gamma}^0 \circ \langle u \rangle\right) \circ \langle u \rangle \\ \left\langle u^2 \right\rangle &= \left(\mathbf{\Gamma} \circ \langle u \rangle\right) \circ \langle u \rangle \\ \left\langle u^3 \right\rangle &= \left(\mathbf{\Gamma} \circ \left(\left(\mathbf{\Gamma} \circ \langle u \rangle\right) \circ \langle u \rangle\right)\right) \circ \langle u \rangle = \left(\mathbf{\Gamma}^2 \circ \langle u \rangle\right) \circ \langle u \rangle \\ \left\langle u^n \right\rangle &= \left(\mathbf{\Gamma}^{n-1} \circ \langle u \rangle\right) \circ \langle u \rangle, \end{aligned} \tag{15}$$

which is useful for expressing polynomial dynamical systems. The following discussions present an approximation of more complex systems in terms of polynomial systems.

TABLE 1. Exponential Function Parameters for Model Validation

t [ms]	0–50	50–100	100–150	150–200
$\langle u \rangle_0$	1	1	$1 + 0.2\sin(20\pi t)$	$1 + 0.2\sin(20\pi t)$
$\langle u \rangle_1$	$0.1e^{\iota\frac{\pi}{3}}$	$0.1e^{\iota\frac{\pi}{3}}$	$0.1e^{\iota\frac{\pi}{3}}$	$0.4e^{\iota\frac{\pi}{3}}$
$\langle u \rangle_2$	0	$0.04e^{\iota\frac{\pi}{6}}$	$0.04e^{\iota\frac{\pi}{6}}$	$0.16e^{\iota\frac{\pi}{6}}$
$\langle u \rangle_3$	0	$0.02e^{\iota\frac{\pi}{12}}$	$0.02e^{\iota\frac{\pi}{12}}$	$0.08e^{\iota\frac{\pi}{12}}$
$\langle u \rangle_4$	0	0	0	$0.04e^{\iota\frac{\pi}{6}}$

C. ON THE MODEL OF EXPONENTIAL FUNCTIONS

Let $u, v \in L^2(\mathbb{R})$, defining the signal v as

$$v := \exp(u). \tag{16}$$

We can then rewrite v relating to the dc component $\langle u \rangle_0$ as

$$v = \exp\left(\langle u \rangle_0\right) \exp\left(u - \langle u \rangle_0\right) = \exp\left(\langle u \rangle_0\right) \exp(w), \tag{17}$$

where $w := u - \langle u \rangle_0$ and $\langle w \rangle = \langle u \rangle|_{\langle u \rangle_0 = 0}$. Thus, (17) can be expressed in terms of its Taylor Series expansion centered at $w = 0$ as

$$\exp(u) = \exp\left(\langle u \rangle_0\right) \sum_{n=0}^{\infty} \frac{w^n}{n!}. \tag{18}$$

From the previous subsection and (18), it is possible to infer that

$$\langle \exp(u) \rangle = e^{\langle u \rangle_0} \left(\hat{h}_0 + \sum_{n=1}^{\infty} \frac{1}{n!} \left(\mathbf{\Gamma}^{n-1} \circ \langle w \rangle\right) \circ \langle w \rangle \right), \tag{19}$$

which can be truncated to ease the analysis and computational burden when employing the presented model in a simulation. Figure 1 shows the behaviour of the approximation given by (19) for an arbitrary signal considering multiple truncation values of the Taylor series to verify the validity of the approximation.

The exponential function serves as a basis for more complex functions, such as trigonometric functions. These can constitute rotations of two-dimensional (2-D) vectors, as in the Park transformation, which is further discussed in the following section.

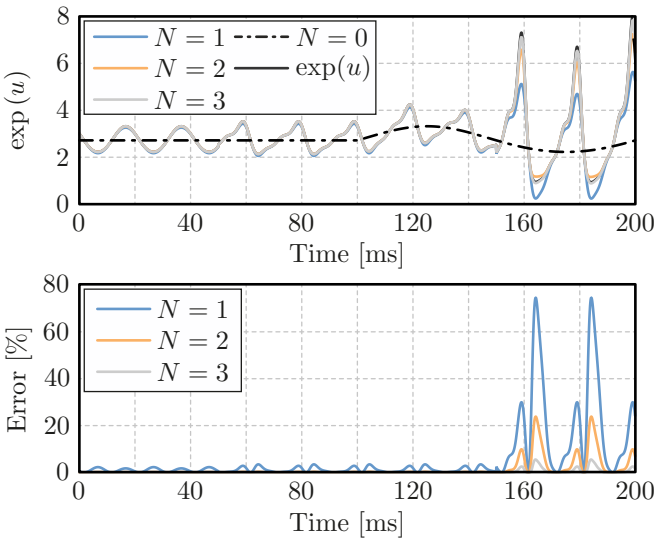

FIGURE 1. Approximation of the exponential function employing the HSS model truncated at the 9^{th} harmonic for multiple Taylor series truncation values (N) with respect to the signal u with amplitudes given by Table 1. The error is defined as the relative error between the real valued function and the projection of the approximation onto the $L^2(\mathbb{R})$ space.

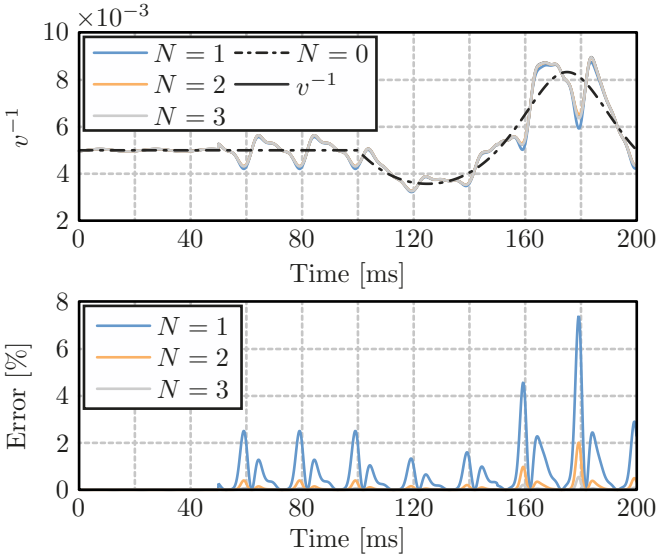

FIGURE 2. Inverse function HSS model approximation truncated at the 9^{th} harmonic for multiple Taylor series truncation values(N) with respect to the signal v given by Table 2. The error is defined as the relative error between the real valued function and the projection of the approximation onto the $L^2(\mathbb{R})$ space.

D. ON THE DIVISION BETWEEN TWO REAL-VALUED SIGNALS

Let $u, v \in L^2(\mathbb{R}), v(t) > 0\ \forall t \in \mathbb{R}$. Also, let $\langle v \rangle_0 > 0$ as the dc component of the denominator, resulting in

$$\frac{u}{v} = \frac{u}{\langle v \rangle_0} \frac{1}{1 + \dfrac{w}{\langle v \rangle_0}}, \tag{20}$$

where $w := v - \langle v \rangle_0$. We can then express (20) in term of its Taylor Series as

$$\frac{u}{v} = \frac{u}{\langle v \rangle_0} \sum_{n=0}^{\infty} \left(\frac{w}{\langle v \rangle_0} \right)^n, \tag{21}$$

assuming that $|w| < \langle v \rangle_0$ due to the series region of convergence. Then, from inspection of (21), we can define the dynamic phasor of the inverse operator as

$$\left\langle \frac{1}{v} \right\rangle = \frac{\hat{h}_0}{\langle v \rangle_0} + \sum_{n=1}^{\infty} \frac{(-1)^n}{\langle v \rangle_0^{n+1}} \left(\mathbf{\Gamma}^{n-1} \circ \langle w \rangle \right) \circ \langle w \rangle \tag{22}$$

and the dynamic phasor of the division between u and v as

$$\boldsymbol{h}_{div}(u, v) := \left\langle \frac{u}{v} \right\rangle = \sum_{n=0}^{\infty} \frac{(-1)^n}{\langle v \rangle_0^{n+1}} \left(\mathbf{\Gamma}^n \circ \langle w \rangle \right) \circ \langle u \rangle . \tag{23}$$

Figures 2 and 3 demonstrate the behaviour of the proposed approximation for the inverse and division of arbitrary signals, validating the proposed approximation.

Another way of modeling the division of two numbers would be through the deconvolution, as in

$$\left\langle \frac{u}{v} \right\rangle = \left(\mathbf{\Gamma}^{-1} \circ \langle v \rangle \right) \circ \langle u \rangle = \left(\mathbf{\Gamma} \circ \langle v \rangle \right)^{-1} \circ \langle u \rangle , \tag{24}$$

since the inverse of the Toeplitz Operator presents a complex analytic calculation, especially for a large number of harmonics. Table 3 compiles a collection of harmonic state-space operations demonstrated in this section.

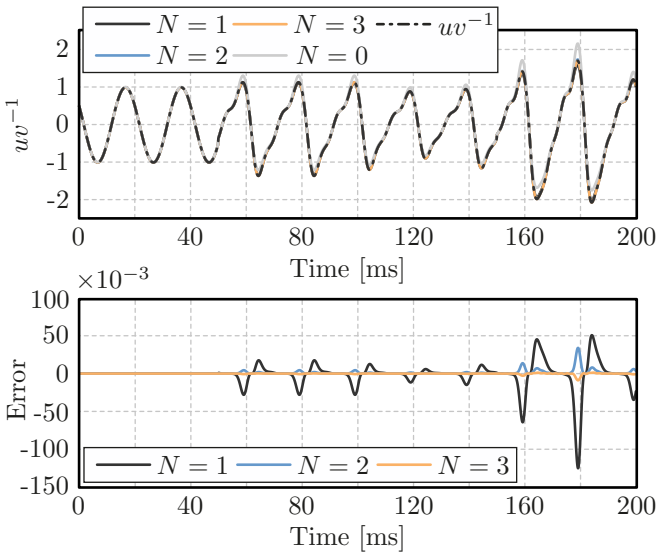

FIGURE 3. Division of two signals employing the inverse function HSS model approximation truncated at the 9^{th} harmonic for multiple Taylor series truncation values (N) with respect to signals u, v given by Table 2. The error is defined as the absolute error between the real valued function and the projection of the approximation onto the $L^2(\mathbb{R})$ space.

The following section demonstrates a spacial rotation of a two dimensional vector as means of computing the Park transformation of a three-phase electrical system.

TABLE 2. Parameters for Division Model Validation

t [ms]	0–50	50–100	100–150	150–200
$\langle u\rangle_0$	0	0	$10\sin(20\pi t)$	$10\sin(20\pi t)$
$\langle u\rangle_1$	$100e^{\iota\frac{\pi}{3}}$	$100e^{\iota\frac{\pi}{3}}$	$100e^{\iota\frac{\pi}{3}}$	$100e^{\iota\frac{\pi}{3}}$
$\langle u\rangle_2$	0	$40e^{\iota\frac{\pi}{6}}$	$40e^{\iota\frac{\pi}{6}}$	$40e^{\iota\frac{\pi}{6}}$
$\langle u\rangle_3$	0	$20e^{\iota\frac{\pi}{12}}$	$20e^{\iota\frac{\pi}{12}}$	$0.20e^{\iota\frac{\pi}{12}}$
$\langle u\rangle_4$	0	0	0	$10e^{\iota\frac{\pi}{6}}$
$\langle v\rangle_0$	200	200	$200+80\sin(20\pi t)$	$200+80\sin(20\pi t)$
$\langle v\rangle_1$	$e^{\iota\frac{\pi}{4}}$	$10e^{\iota\frac{\pi}{4}}$	$10e^{\iota\frac{\pi}{4}}$	$10e^{\iota\frac{\pi}{4}}$
$\langle v\rangle_2$	0	$5e^{\iota\frac{\pi}{6}}$	$5e^{\iota\frac{\pi}{6}}$	$50e^{\iota\frac{\pi}{6}}$
$\langle v\rangle_3$	0	$2.5e^{\iota\frac{\pi}{12}}$	$2.5e^{\iota\frac{\pi}{12}}$	$2.5e^{\iota\frac{\pi}{12}}$
$\langle v\rangle_4$	0	0	0	$e^{\iota\frac{\pi}{6}}$

III. PARK TRANSFORMATION THROUGH A HARMONIC STATE-SPACE APPROACH

A. SPACIAL ROTATION OF A TWO-DIMENSIONAL VECTOR

Let $\mathbf{u}_{abc}\in\mathbb{R}^3$ a generic three-phase electrical quantity. Let us also define a complex voltage signal $\bar{u}$, which results from the projection of a three-phase electrical quantity vector onto the $\alpha\beta$ plane through the Clarke Transformation as in

$$\bar{u} := \begin{bmatrix}1 & e^{-\iota\frac{2}{3}\pi} & e^{\iota\frac{2}{3}\pi}\end{bmatrix}\mathbf{u}_{abc} \tag{25}$$

in its complex form, or

$$\mathbf{u} := (\Re\{\bar{u}\},\Im\{\bar{u}\}) = (u_\alpha, u_\beta) \tag{26}$$

in its real form. We can then write $\bar{u}\in L^2(\mathbb{C})$ such that

$$\begin{aligned}\bar{u} &= \sum_{n=-\infty}^{\infty}\langle u_\alpha\rangle_n e^{\iota n\omega t} + \iota\langle u_\beta\rangle_n e^{\iota n\omega t}\\ &= \langle u_\alpha\rangle_0 + \iota\langle u_\beta\rangle_0\\ &\quad + 2\sum_{n=1}^{\infty}\Re\left\{\langle u_\alpha\rangle_n e^{\iota n\omega t}\right\} + \iota\Re\left\{\langle u_\beta\rangle_n e^{\iota n\omega t}\right\}.\end{aligned} \tag{27}$$

Thus, the dynamic phasor of each component can be written as

$$\langle\mathbf{u}\rangle_n = (\langle u_\alpha\rangle_n, \langle u_\beta\rangle_n)\in\ell^2(\mathbb{C}^2), \forall n\in\mathbb{Z}.$$

From this, let us define the the Park transformation as the projection of $\bar{u}$ onto the rotating frame $e^{\iota\theta_\delta}$ as

$$\bar{u}_{dq} := \bar{u}e^{-\iota\theta_\delta} = u_d + \iota u_q, \tag{28}$$

where

$$\theta_\delta = \int_0^t \omega \mathrm{d}t + \delta.$$

We can also write $\mathbf{u}_{dq} := (u_d, u_q)$ as a real-valued vector.

Hence, the rotation of a complex valued signal solves for (29) in the time-domain, which is defined at the top of the following page, and results in two frequency components related to the adjacent harmonics dependent on the positive and negative sequences. Subsequently, we can define two distinct dynamic phasors the these adjacent frequencies of the dq components as

$$\langle\mathbf{u}_{dq,k}\rangle := (\langle\mathbf{u}_{dq}\rangle_{k+1}, \langle\mathbf{u}_{dq}\rangle_{k-1})\in\ell^2(\mathbb{C}^4), \forall n\in\mathbb{Z} \tag{30}$$

where

$$\langle\mathbf{u}_{dq}\rangle_k := (\langle u_d\rangle_k, \langle u_d\rangle_k)\in\ell^2(\mathbb{C}^2), \forall k\in\mathbb{Z}.$$

Thus, we can define a linear map $\boldsymbol{f}\in\mathcal{L}(\mathbb{C}^2,\mathbb{C}^4)$, such that $\langle\mathbf{u}_{dq,k}\rangle = \boldsymbol{f}\circ\langle\mathbf{u}\rangle_k$ as

$$[\boldsymbol{f}] = \frac{1}{2}\begin{bmatrix} e^{\iota\delta} & -\iota e^{\iota\delta}\\ \iota e^{\iota\delta} & e^{\iota\delta}\\ e^{-\iota\delta} & \iota e^{-\iota\delta}\\ -\iota e^{-\iota\delta} & e^{-\iota\delta}\end{bmatrix}, \tag{31}$$

with $\mathrm{rank}(\boldsymbol{f}) = 2$. We can also define the inverse linear map $\boldsymbol{f}^+$ through the Moore-Penrose pseudo-inverse of $\boldsymbol{f}$ as

$$\left[\boldsymbol{f}^+\right] = \frac{1}{2}\begin{bmatrix} e^{-\iota\delta} & -\iota e^{-\iota\delta} & e^{\iota\delta} & \iota e^{\iota\delta}\\ \iota e^{-\iota\delta} & e^{-\iota\delta} & -\iota e^{\iota\delta} & e^{\iota\delta}\end{bmatrix}, \tag{32}$$

since $\boldsymbol{f}$ is not bijective. Note that $\boldsymbol{f}^+ = \boldsymbol{f}^H$.

We can then decompose $\boldsymbol{f}$ into two different components $\boldsymbol{f}_-, \boldsymbol{f}_+\in\mathcal{L}(\mathbb{C}^2,\mathbb{C}^2)$, the first one restricted to $\langle\mathbf{u}_{dq}\rangle_{n-1}$ and the other restricted to $\langle\mathbf{u}_{dq}\rangle_{n+1}$, defined as

$$[\boldsymbol{f}_+] = \frac{1}{2}\begin{bmatrix}1 & -\iota\\ \iota & 1\end{bmatrix}e^{\iota\delta}, \quad [\boldsymbol{f}_-] = \frac{1}{2}\begin{bmatrix}1 & \iota\\ -\iota & 1\end{bmatrix}e^{-\iota\delta}, \tag{33}$$

which can be called the negative and positive sequence functionals, respectively. We can then write the signal k^{th} harmonic components in dq coordinates as

$$\langle\mathbf{u}_{dq}\rangle_k = \boldsymbol{f}_+\circ\langle\mathbf{u}\rangle_{k-1} + \boldsymbol{f}_-\circ\langle\mathbf{u}\rangle_{k+1} \tag{34}$$

Let us define $\langle\mathbf{u}\rangle := (\langle\mathbf{u}\rangle_k)_{k=-\infty}^{\infty}$ as the set of DPs in $\alpha\beta$ coordinates and $\langle\mathbf{u}_{dq}\rangle := (\langle\mathbf{u}_{dq}\rangle_k)_{k=-\infty}^{\infty}$ the set of DP for dq coordinates. Consequently, we can express the linear map $\boldsymbol{g}\in\mathcal{L}(\ell^2(\mathbb{C}^2),\ell^2(\mathbb{C}^2))$ such that $\langle\mathbf{u}_{dq}\rangle = \boldsymbol{g}\circ\langle\mathbf{u}\rangle$ as

$$[\boldsymbol{g}] = \begin{bmatrix} \ddots & & & & & & \\ \ddots & f_- & & & & & \\ \ddots & 0 & f_- & & & & \\ & f_+ & 0 & f_- & & & \\ & & f_+ & 0 & f_- & & \\ & & & f_+ & 0 & f_- & \\ & & & & \ddots & \ddots & \ddots\end{bmatrix} \tag{35}$$

which can be truncated for a given number of harmonics. Note that $\boldsymbol{f}_+ = \boldsymbol{f}_-^*$, thus the equality given by

$$\langle\mathbf{u}_{dq}\rangle_{-h} = \langle\mathbf{u}_{dq}\rangle_h^* \tag{36}$$

is still valid. The linear map $\boldsymbol{\Psi}_2$ defined in (10) can also be employed as means of obtaining a real valued system.

With this, we can write the spacial rotation of a two-dimensional signal in the Harmonic State-Space with respect to an arbitrary angle δ, and consequently the Park transformation, as

$$\begin{aligned}\langle\mathbf{u}_{dq}\rangle &= \boldsymbol{g}(\delta)\circ\langle\mathbf{u}\rangle\\ \langle\mathbf{u}\rangle &= \boldsymbol{g}^H(\delta)\circ\langle\mathbf{u}_{dq}\rangle.\end{aligned} \tag{37}$$

Figure 4 shows a comparison for arbitrary $\mathbf{u}$ and δ using the time-variant and HSS based approaches to compute the Park-transformation with a time-variant angle, which validates the previously described equations. In this case, a time-variant

$$
\begin{aligned}
u_d = \frac{1}{4}\sum_{k=-\infty}^{\infty} \big(&\left(\Re\left\{\langle u_\alpha\rangle_k\right\} + \Im\left\{\langle u_\beta\rangle_k\right\}\right)\cos\left((k+1)\omega t+\delta\right) + \left(-\Im\left\{\langle u_\alpha\rangle_k\right\} + \Re\left\{\langle u_\beta\rangle_k\right\}\right)\sin\left((k+1)\omega t+\delta\right) \\
&+ \left(\Re\left\{\langle u_\alpha\rangle_k\right\} - \Im\left\{\langle u_\beta\rangle_k\right\}\right)\cos\left((k-1)\omega t-\delta\right) + \left(\Im\left\{\langle u_\alpha\rangle_k\right\} + \Re\left\{\langle u_\beta\rangle_k\right\}\right)\sin\left((k-1)\omega t-\delta\right)\big) \\
u_q = \frac{1}{4}\sum_{k=-\infty}^{\infty} \big(&\left(-\Im\left\{\langle u_\alpha\rangle_k\right\} + \Re\left\{\langle u_\beta\rangle_k\right\}\right)\cos\left((k+1)\omega t+\delta\right) + \left(-\Re\left\{\langle u_\alpha\rangle_k\right\} - \Im\left\{\langle u_\beta\rangle_k\right\}\right)\sin\left((k+1)\omega t+\delta\right) \\
&+ \left(\Im\left\{\langle u_\alpha\rangle_k\right\} + \Re\left\{\langle u_\beta\rangle_k\right\}\right)\cos\left((k-1)\omega t-\delta\right) + \left(\Re\left\{\langle u_\alpha\rangle_k\right\} - \Im\left\{\langle u_\beta\rangle_k\right\}\right)\sin\left((k-1)\omega t-\delta\right)\big)
\end{aligned}
\tag{29}
$$

δ was employed, as a detailed analysis of δ is explored in the following subsection.

From (34), we can also define the $\boldsymbol{g}_{j,k}, \forall j \in \{d,q\}$ such that

$$
\begin{aligned}
\langle \mathbf{u}_d\rangle_k &= \frac{1}{2}\begin{bmatrix} e^{\iota\delta} & -\iota e^{\iota\delta} & e^{-\iota\delta} & \iota e^{-\iota\delta}\end{bmatrix}\begin{bmatrix}\langle \mathbf{u}\rangle_{k-1}\\ \langle \mathbf{u}\rangle_{k+1}\end{bmatrix} = \boldsymbol{g}_{d,k}\circ\langle u\rangle \\
\langle \mathbf{u}_q\rangle_k &= \frac{1}{2}\begin{bmatrix} \iota e^{\iota\delta} & e^{\iota\delta} & -\iota e^{-\iota\delta} & e^{-\iota\delta}\end{bmatrix}\begin{bmatrix}\langle \mathbf{u}\rangle_{k-1}\\ \langle \mathbf{u}\rangle_{k+1}\end{bmatrix} = \boldsymbol{g}_{q,k}\circ\langle u\rangle
\end{aligned}
\tag{38}
$$

as means of obtaining a single harmonic component.

However, (37) still considers a time-variant angle $\delta \in \mathbb{R}$, hence the following subsection aims to obtain a large-signal model in terms of the harmonic components of δ.

B. PARK TRANSFORMATION LARGE-SIGNAL HSS MODEL

Let $\delta \in L^2(\mathbb{R})$ such that

$$
\delta := \sum_{k=-\infty}^{\infty} \langle\delta\rangle_k e^{\iota k\omega t} \tag{39}
$$

be given by the projection of the DPs onto the real plane, which in turn defines

$$
\begin{aligned}
\bar{\xi} &:= \exp\left\{-\iota\delta\right\} \\
&:= \exp\left\{-\iota\sum_{n=-\infty}^{\infty}\langle\delta\rangle_n e^{\iota n\omega t}\right\}
\end{aligned}
\tag{40}
$$

as a complex rotation dependent on the dynamic phasor of the angle displacement. We can then apply the procedure

TABLE 3. Dynamic Phasor Function Approximations

Operation	Symbol	Expression
Multiplication	$\langle uv\rangle$	$(\boldsymbol{\Gamma}\circ\langle u\rangle)\circ\langle v\rangle$
Exponentiation	$\langle u^n\rangle$	$\left(\boldsymbol{\Gamma}^{n-1}\circ\langle u\rangle\right)\circ\langle u\rangle = (\boldsymbol{\Gamma}\circ\cdots\circ(\boldsymbol{\Gamma}\circ\langle u\rangle)\circ\langle u\rangle)\circ\langle u\rangle$
Exponential Function	$\boldsymbol{h}_{\exp}(\langle u\rangle)$	$e^{\langle u\rangle_0}\left(\hat{h}_0 + \sum_{n=1}^{\infty}\frac{1}{n!}\left(\boldsymbol{\Gamma}^{n-1}\circ\langle u\rangle\Big\vert_{\langle u\rangle_0=0}\right)\circ\langle u\rangle\Big\vert_{\langle u\rangle_0=0}\right)$
Division	$\boldsymbol{h}_{div}(u,v)$	$\sum_{n=0}^{\infty}\frac{(-1)^n}{\langle v\rangle_0^{n+1}}\left(\boldsymbol{\Gamma}^n\circ\langle v\rangle\Big\vert_{\langle v\rangle_0=0}\right)\circ\langle u\rangle$
Synchronous Rotation	$\boldsymbol{g}_\delta(\langle\delta\rangle_0)$	See (33) and (35)
Park Transformation	$\boldsymbol{h}_\delta(\delta)$	$\sum_{n=0}^{\infty}\frac{1}{n!}\left(\left(\boldsymbol{\Gamma}^n\circ\langle\delta\rangle\vert_{\langle\delta\rangle_0=0}\right)\otimes\mathbf{I}_2\right)\circ\boldsymbol{g}_\delta\left(\langle\delta\rangle_0 + n\frac{\pi}{2}\right)$
d-Axis Component	$\boldsymbol{h}_d(\delta)$	$(\mathbf{I}_{N_h}\otimes[1\quad 0])\circ\boldsymbol{h}_\delta(\delta)$
q-Axis Component	$\boldsymbol{h}_q(\delta)$	$(\mathbf{I}_{N_h}\otimes[0\quad 1])\circ\boldsymbol{h}_\delta(\delta)$
PLL Feedback	$\boldsymbol{h}_{pll}(\mathbf{u}_{\alpha\beta},\delta)$	$\boldsymbol{h}_{div}\left(\boldsymbol{h}_q(\delta)\circ\mathbf{u}_{\alpha\beta}, \boldsymbol{h}_d(\delta)\circ\mathbf{u}_{\alpha\beta}\right)$
VCO Signal	$\boldsymbol{h}_{vco}(\langle\delta\rangle)$	$\left(\mathbf{I}_\infty\otimes\begin{bmatrix}1 & 0\end{bmatrix}\right)\circ\boldsymbol{h}_d^H(\delta)\circ\hat{h}_0$

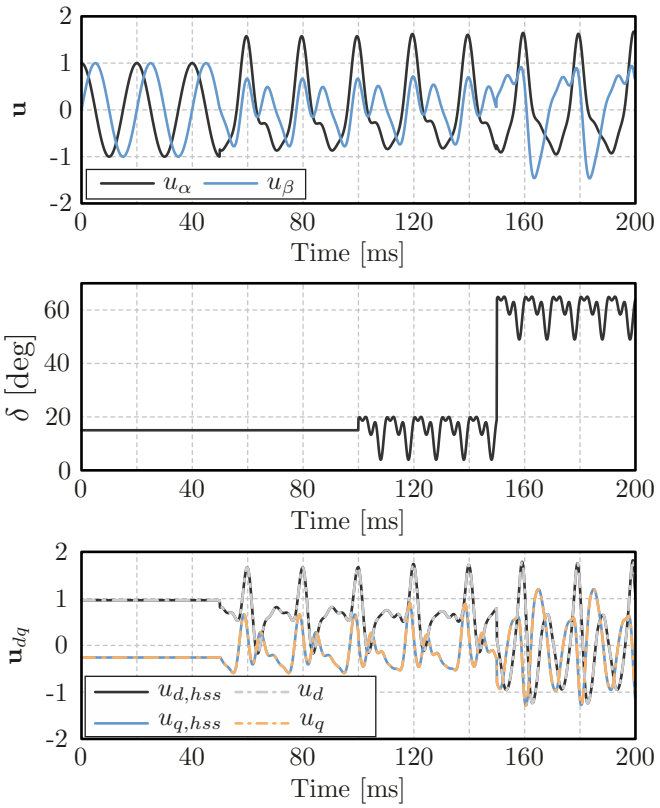

FIGURE 4. HSS model validation of the spatial rotation of a 2-D time-variant vector $\mathbf{u} = (u_\alpha, u_\beta)$ by the time varying angle $\delta \in L^2(\mathbb{R})$ defined by Table 4.

TABLE 4. Parameters for Park Transformation Model Validation

t [ms]	0–50	50–100	100–150	150–200
$\langle u_\alpha \rangle_0$	0	0	$0.05\sin(20\pi t)$	$0.05\sin(20\pi t)$
$\langle u_\alpha \rangle_1$	0.5	0.5	0.5	0.5
$\langle u_\alpha \rangle_2$	0	$0.2e^{\iota\frac{\pi}{6}}$	$0.2e^{\iota\frac{\pi}{6}}$	$0.2e^{\iota\frac{\pi}{6}}$
$\langle u_\alpha \rangle_3$	0	$0.1e^{\iota\frac{\pi}{12}}$	$0.1e^{\iota\frac{\pi}{12}}$	$0.1e^{\iota\frac{\pi}{12}}$
$\langle u_\alpha \rangle_4$	0	0	0	$0.05e^{\iota\frac{\pi}{6}}$
$\langle u_\beta \rangle_0$	0	0	$0.05\sin(20\pi t)$	$0.05\sin(20\pi t)$
$\langle u_\beta \rangle_1$	$0.5e^{-\iota\frac{\pi}{2}}$	$0.2e^{-\iota\frac{2\pi}{5}}$	$0.2e^{-\iota\frac{2\pi}{5}}$	$0.5e^{\iota\frac{\pi}{2}}$
$\langle u_\beta \rangle_2$	0	$0.2e^{\iota\frac{\pi}{6}}$	$0.2e^{\iota\frac{\pi}{6}}$	$0.2e^{\iota\frac{\pi}{6}}$
$\langle u_\beta \rangle_3$	0	$0.1e^{\iota\frac{\pi}{12}}$	$0.1e^{\iota\frac{\pi}{12}}$	$0.1e^{\iota\frac{\pi}{12}}$
$\langle u_\beta \rangle_4$	0	0	0	$0.05e^{\iota\frac{\pi}{6}}$
$\langle \delta \rangle_0$	$\frac{\pi}{12}$	$\frac{\pi}{12}$	$\frac{\pi}{12}$	$\frac{\pi}{3}$
$\langle \delta \rangle_2$	0	0	$\frac{\pi}{72}e^{-\iota\frac{\pi}{2}}$	$\frac{\pi}{72}e^{-\iota\frac{\pi}{2}}$
$\langle \delta \rangle_4$	0	0	$\frac{\pi}{100}e^{-\iota\frac{\pi}{3}}$	$\frac{\pi}{100}e^{-\iota\frac{\pi}{3}}$
$\langle \delta \rangle_6$	0	0	$\frac{\pi}{120}e^{\iota\frac{\pi}{5}}$	$\frac{\pi}{120}e^{\iota\frac{\pi}{5}}$

adopted in (18) to (40), which results in

$$\begin{aligned}\bar{\xi} &= \exp\left(-\iota\langle\delta\rangle_0\right)\sum_{n=0}^{\infty}\frac{(\iota w)^n}{n!}\\ &= \sum_{n=0}^{\infty}\exp\left(-\iota\left(\langle\delta\rangle_0 + n\frac{\pi}{2}\right)\right)\frac{w^n}{n!},\end{aligned} \tag{41}$$

where $w = \delta - \langle\delta\rangle_0$. Note that each term of the sum corresponds to a rotation of a two dimensional signal, with its formulation given by (47). From inspection of (19), we can write $\langle \mathbf{u}_{dq} \rangle := \langle \bar{u}\bar{\xi} \rangle$ as

$$\begin{aligned}\langle \mathbf{u}_{dq} \rangle = &\sum_{n=0}^{\infty}\frac{1}{n!}\left(\left(\mathbf{\Gamma}^n \circ \langle\delta\rangle|_{\langle\delta\rangle_0=0}\right)\otimes\mathbf{I}_2\right)\circ\\ &\circ\boldsymbol{g}\left(\langle\delta\rangle_0 + n\frac{\pi}{2}\right)\circ\langle u\rangle\\ =:&\ \boldsymbol{h}_\delta\left(\mathbf{u},\delta\right).\end{aligned} \tag{42}$$

Since $\langle \mathbf{u}_{dq} \rangle$ concatenates the d and q axis, we can define the linear maps $\mathbf{T}_d, \mathbf{T}_q \in \mathcal{L}(\mathbb{C}^{2n_h}, \mathbb{C}^{n_h})$ as

$$[\mathbf{T}_d] := \mathbf{I}_{n_h} \otimes \begin{bmatrix}1 & 0\end{bmatrix}, \quad [\mathbf{T}_q] := \mathbf{I}_{n_h} \otimes \begin{bmatrix}0 & 1\end{bmatrix}, \tag{43}$$

such that $\langle \mathbf{u}_j \rangle = \mathbf{T}_j \circ \langle \mathbf{u}_{dq} \rangle, \forall j \in \{d, q\}$, which leads to

$$\boldsymbol{h}_j := \mathbf{T}_j \circ \boldsymbol{h}_\delta, \forall j \in \{d, q\} \tag{44}$$

as means of directly obtaining each dq-axis component.

Figure 5 demonstrates the model validation for arbitrary $\langle\delta\rangle$ and $\langle u\rangle$, with explicit values given by 4.

IV. SYNCHRONOUS-REFERENCE FRAME PHASE-LOCKED LOOP MODEL

Let the input signal $u \in \mathbb{C}$ be defined by (27). Hence we can write the SRF-PLL dynamic equations according to

$$\begin{cases} \upsilon_{pll} = \dfrac{\Im\left\{\bar{u}e^{-\iota\theta_\delta}\right\}}{\Re\left\{\bar{u}e^{-\iota\theta_\delta}\right\}} \\ \dot{\mathbf{x}}_{pll} = \mathbf{A}_{pll}\mathbf{x}_{pll} + \mathbf{B}_{pll}\upsilon_{pll} \\ \dot{\delta} = \mathbf{C}_{pll}\mathbf{x}_{pll} + \mathbf{D}_{pll}\upsilon_{pll} \\ \theta_\delta = \omega_g t + \delta \\ \hat{\omega} = \dot{\delta} + \omega_g \end{cases}, \tag{45}$$

where ω_g is the PLL feedforward frequency, which can be fixed or adaptive as means of improving the PLL performance, and the set $\mathcal{M}_{pll} := \{\mathbf{A}_{pll}, \mathbf{B}_{pll}, \mathbf{C}_{pll}, \mathbf{D}_{pll}\}$ is the state-space model of the loop filter. The loop filter was chosen arbitrarily in a first moment, with its block diagram shown in Fig. 6, while considering the input normalization given by the d-axis component. A more thorough approach would be to normalize the imaginary component as in

$$\upsilon'_{pll} = \frac{\Im\left\{\bar{u}e^{-\iota\theta_\delta}\right\}}{|\bar{u}e^{-\iota\theta_\delta}|} = \frac{\Im\left\{\bar{u}e^{-\iota\theta_\delta}\right\}}{\|\mathbf{u}\|_2}, \tag{46}$$

solving for the normalization approach described by (45) when $\Re\{\bar{u}_{dq}\} \gg \Im\{\bar{u}_{dq}\}$. This is mostly true since the synchronism loop forces $\Im\{\bar{u}_{dq}\}$ to a null value, whereas $\Re\{\bar{u}_{dq}\}$ converges to $\|u\|_2$ if no disturbances in the synchronism loop are considered.

If the description of the input u belongs to a dynamic system in dq components, while leaving out harmonics of the electrical quantities, the analysis can be simplified, since u_q is not time-varying, as shown in [8]. However, if the model description for u is time-varying, the approach presented in the previous sections can be employed as means to obtain a large-signal time-invariant nonlinear model. From this, we

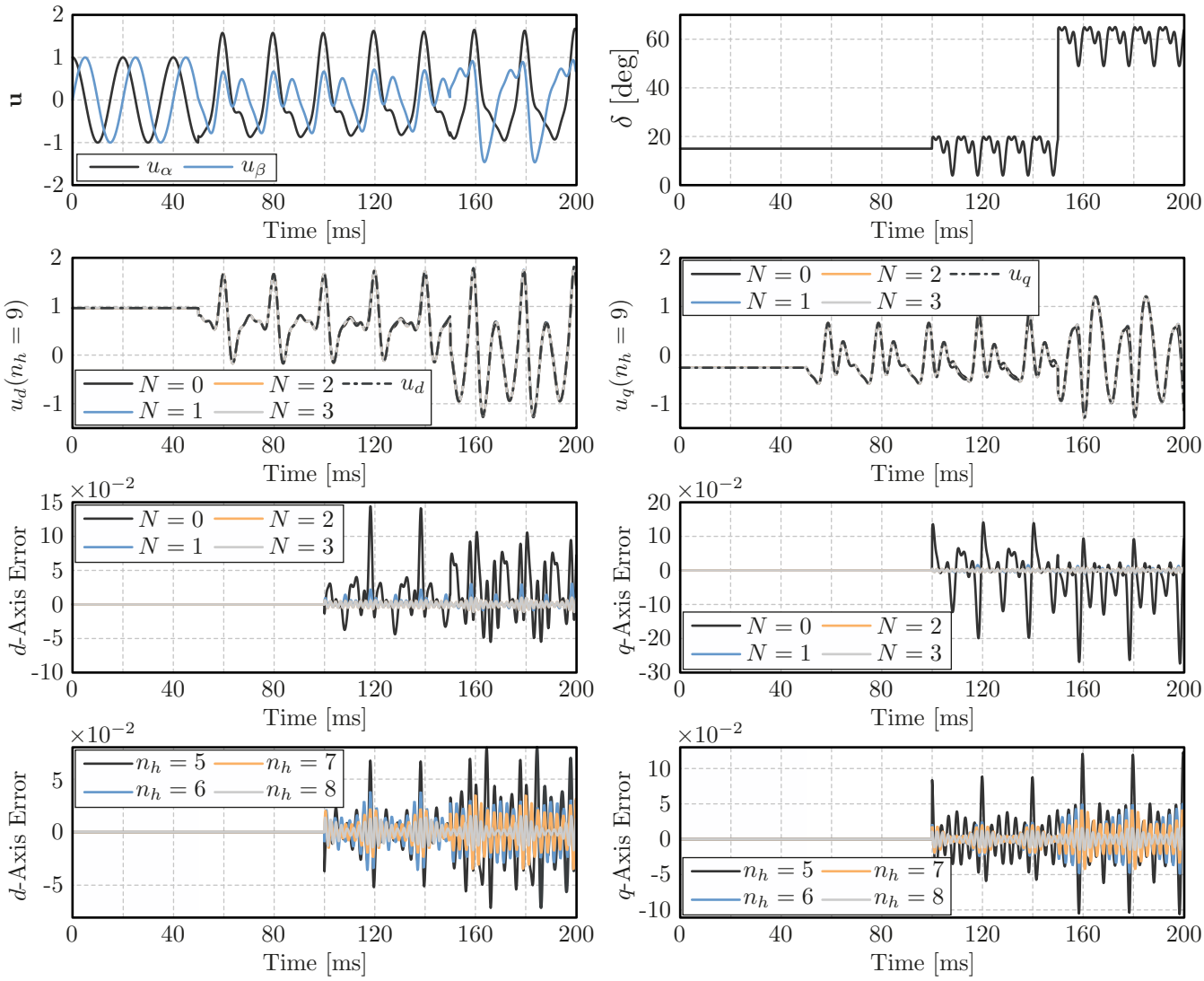

FIGURE 5. Validation of the harmonic domain-based Park Transformation model for arbitrary signals $\langle\delta\rangle$ and $\langle u\rangle$ with the dynamic phasor amplitudes given in Table 4. The error is defined as the absolute error between the real valued function and the projection of the approximation onto the $L^2(\mathbb{R})$ space.

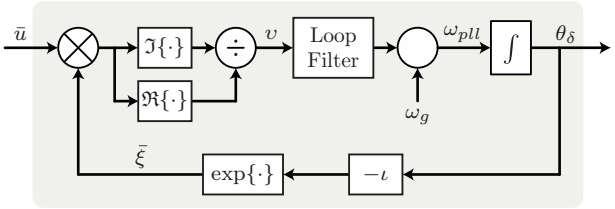

FIGURE 6. Block diagram of the SRF-PLL with a generic Loop Filter.

can adopt two different approaches, which are described in the sequence.

A. DISCUSSION ON SMALL-SIGNAL ANALYSIS

In a first moment, we can assume that $\|\delta\|$ is small enough such that the linearization for $\bar{\delta} = \delta|_{\dot{\delta}=0}$ for a certain $\bar{\delta} \in [0, 2\pi)$ is valid, hence we can write u_{dq} as

$$u_{dq} \approx \sqrt{2}\,\|\langle u\rangle_1\|_2 \left(1, \bar{\delta} + \tilde{\delta}\right), \tag{47}$$

where $\tilde{\delta} = \delta - \bar{\delta}$ and the approximation for u_d is the grid or power converter ac rated voltage, and a small enough $\bar{\delta}$ which can be modelled as a disturbance. Note that if (47) is applied to (45), we have that both systems are coupled by the disturbance $\bar{\delta}$, which has no explicit formulation, i.e., the

TABLE 5. SRF-PLL Loop Filter Parameters

Description	Parameter	Value
Feedforward Frequency	ω_g	$2\pi 50$ rad/s
Sampling frequency	Δt	100 μs
PI Proportional Gain	k_p	56.2
PI Integral Gain	k_i	1784

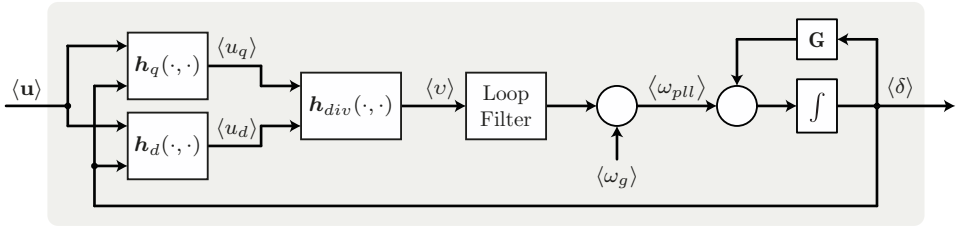

FIGURE 7. Block diagram of the proposed SRF-PLL model with a generic loop filter base on the dynamic equations described in (49).

TABLE 6. Parameters for Park Transformation Model Validation

t [ms]	0–160	160–480	480–800
$\langle u_\alpha \rangle_1$	50	50	50
$\langle u_\alpha \rangle_2$	0	$5e^{\iota\frac{\pi}{6}}$	$5e^{\iota\frac{\pi}{6}}$
$\langle u_\alpha \rangle_3$	0	$2.5e^{\iota\frac{\pi}{12}}$	$2.5e^{\iota\frac{\pi}{12}}$
$\langle u_\alpha \rangle_4$	0	0	$1.25e^{\iota\frac{\pi}{6}}$
$\langle u_\beta \rangle_1$	$50e^{-\iota\frac{\pi}{2}}$	$20e^{-\iota\frac{2\pi}{5}}$	$50e^{-\iota\frac{\pi}{2}}$
$\langle u_\beta \rangle_2$	0	$5e^{\iota\frac{\pi}{6}}$	$5e^{\iota\frac{\pi}{6}}$
$\langle u_\beta \rangle_3$	0	$2.5e^{\iota\frac{\pi}{12}}$	$2.5e^{\iota\frac{\pi}{12}}$
$\langle u_\beta \rangle_4$	0	0	$1.25e^{\iota\frac{\pi}{6}}$

synchronism electrical quantity $\mathbf{u}$ and reference generation dynamic systems are mostly independent. Thus, equation (47) can be used in conjunction with the concepts of DP or HSS and the Toeplitz operator to obtain a description of the system, which is mostly valid as $\bar{\delta}$ approaches zero, corroborating the small signal analysis presented in [12], [20], [21].

However, a correct choice of $\bar{\delta}$ is necessary to define the correct point of operation, as means of coupling the outer system that defines $\mathbf{u}$ and the synchronism loop small-signal model, which is discussed in [22] as the initial angle problem. Nevertheless, such approach is inaccurate, as $\bar{\delta}$ should be the solution of the system at its fixed point. Furthermore, the existence of this fixed point is not guaranteed due to the nonlinear characteristic of said system. For example, an instability of the PLL control loop leads to a chaotic orbit (which can be periodic), as the feedback is bounded.

On a side note, the phase angle and the voltage amplitude employed for the normalization of the synchronism electrical quantity is extremely dependent on the active and reactive power processed by power converters under weak-grid conditions. Hence, this linearization is not adequate for the characterization of the fixed points as means of asserting the system's stability under weak grid conditions.

Concurrently, the frequency coupling terms given by higher order terms of the Taylor series expressed in (42) will lead to a synchronization deviation such that the estimation error e_δ does in fact converges to a value $\epsilon \in \mathbb{R}$ under distorted grid conditions. This effect can also be amplified by the normalisation of the PLL input, as the approximation given by (23) can also lead to a coupling between two distinct harmonics and $\langle \delta \rangle_0$.

B. SRF-PLL LARGE-SIGNAL MODEL APPROXIMATION

Another alternative is to consider the nonlinear characteristic of the SRF-PLL equations in (45). From (42), (44) and (23), we can employ the previously defined linear maps $\boldsymbol{h}_d, \boldsymbol{h}_q$, as well as the division operator $\boldsymbol{h}_{div}$ as means of computing the normalization. Thus, the set of DPs of v_{pll} can be written as a function of the set of dynamic phasors of the input $\langle \mathbf{u} \rangle$ and the estimated displacement angle $\langle \delta \rangle$ according to

$$\boldsymbol{h}_{pll}(\mathbf{u}, \delta) := \langle v_{pll} \rangle = \boldsymbol{h}_{div}\left(\boldsymbol{h}_q(\mathbf{u}, \delta), \boldsymbol{h}_d(\mathbf{u}, \delta)\right). \tag{48}$$

Consequently, the PLL dynamic equations can be expressed as

$$\begin{cases} D_t \langle \mathbf{x}_{pll} \rangle = \left(\mathbf{I}_{N_h} \otimes \mathbf{A}_{pll} - \operatorname{diag}(\mathfrak{H}) \otimes \iota\omega \mathbf{I}_{n_{pll}}\right) \langle \mathbf{x}_{pll} \rangle \\ \qquad\qquad + \left(\mathbf{I}_{N_h} \otimes \mathbf{B}_{pll}\right) \boldsymbol{h}_{pll}(\mathbf{u}, \delta) \\ D_t \langle \delta \rangle = \left(\mathbf{I}_{N_h} \otimes \mathbf{C}_{pll}\right) \langle \mathbf{x}_{pll} \rangle + \left(\mathbf{I}_{N_h} \otimes \mathbf{D}_{pll}\right) \boldsymbol{h}_{pll}(\mathbf{u}, \delta) \\ \qquad\qquad + \langle \omega_g \rangle - \omega \hat{h}_0 - \iota\omega \operatorname{diag}(\mathfrak{H}) \langle \delta \rangle \end{cases}, \tag{49}$$

where $\mathfrak{H}$ is the set of harmonics considered in the analysis and $n_h := \dim(\mathfrak{H})$. A block diagram of the proposed HSS model is presented in Fig. 7.

A simplification can be adopted as means of reducing the complexity of the model presented in (49) letting $\langle \delta \rangle_j = 0, \forall j \neq 0$, while also normalizing the PLL input signal by the dc component of the d-axis signal, resulting in

$$\begin{cases} D_t \langle \mathbf{x}_{pll} \rangle_0 = \mathbf{A}_{pll} \langle \mathbf{x}_{pll} \rangle_0 + \mathbf{B}_{pll} \dfrac{\boldsymbol{g}_{q,0}(\langle \delta \rangle_0) \circ \langle \mathbf{u} \rangle}{\boldsymbol{g}_{d,0}(\langle \delta \rangle_0) \circ \langle \mathbf{u} \rangle} \\ D_t \langle \delta \rangle_0 = \mathbf{C}_{pll} \langle \mathbf{x}_{pll} \rangle_0 + \mathbf{B}_{pll} \dfrac{\boldsymbol{g}_{q,0}(\langle \delta \rangle_0) \circ \langle \mathbf{u} \rangle}{\boldsymbol{g}_{d,0}(\langle \delta \rangle_0) \circ \langle \mathbf{u} \rangle} \\ \qquad\qquad + \langle \omega_g \rangle_0 - \omega \end{cases}, \tag{50}$$

which is mostly valid when employing control techniques to mitigate disturbances of the electrical quantities signals mainly caused by negative sequence components and harmonic distortions. Note that $g(\delta)$ presents a bounded behaviour for the feedback, since

$$\|g(\delta)\|_2 = \|\langle \mathbf{u}_{dq} \rangle\|_2 \, \|\langle \mathbf{u} \rangle\|_2^{-1} = 1, \quad \forall \mathbf{u} \neq \mathbf{0}, \delta \in \mathbb{R}, \tag{51}$$

which in turn takes into account an eventual loss-of-lock and the possibility of a re-synchronization. This poses as an advantage of truncating (35) at the first term, otherwise the harmonic content of δ can lead to a positive feedback, i.e,

a reduction in the stability margin of the PLL control loop. This simplified model can also be employed for stability analysis of power converter systems for the investigation and identification of loss-of-lock and subharmonics, especially when operating under weak-grid conditions.

Another advantage of this procedure is that the dynamic phasor frequency was written as a system disturbance, with the assumption that $\dot{\omega}$ vanishes, hence frequency disturbances are also fed back into the dynamic system, which is useful for obtaining frequency dependent models for power system analysis. The following section presents a numerical simulation of the proposed model while employing a traditional control strategy as means of validating the proposed model and assert the dependence of the proposed model with respect to the truncation of the infinite dimensional model, which is related to the number of harmonics and terms of the Taylor series expansion.

C. Numerical Example

Assume the loop filter as a PI controller, such that

$$\mathbf{A}_{pll} = 0, \quad \mathbf{B}_{pll} = 1, \quad \mathbf{C}_{pll} = k_i, \quad \mathbf{D}_{pll} = k_p, \qquad (52)$$

where k_p and k_i are the proportional and integral gains, respectively. Hence, equation (49) can be rewritten as

$$\begin{cases} D_t \langle \mathbf{x}_{pll} \rangle = -\iota\omega \mathrm{diag}\left(\mathfrak{H}\right) \langle \mathbf{x}_{pll} \rangle + \boldsymbol{h}_{pll}(\mathbf{u}, \delta) \\ D_t \langle \delta \rangle = -\iota\omega \mathrm{diag}\left(\mathfrak{H}\right) \langle \delta \rangle + k_i \langle \mathbf{x}_{pll} \rangle + k_p \boldsymbol{h}_{pll}(\mathbf{u}, \delta) \, . \\ \qquad\qquad + \langle \omega_g \rangle - \omega \end{cases} \qquad (53)$$

The truncated model has three degrees of freedom: N_h, N_{div} and N_g, related to the number of harmonics of the set $\mathfrak{H}$, the number of Taylor series terms of the normalization procedure and to the number of Taylor series terms of the 2-D rotation operation, respectively. An adequate choice of these parameters is critical due to the increased complexity related to the number of operations. Let n_h the number of harmonics such that $\mathfrak{H} = \{h \in \mathbb{Z} : -n_h \leq h \leq n_h\}$, which leads to $N_h = 2n_h + 1$. Based on this, the simulation results presented in Fig. 8 demonstrates the validation of the SRF-PLL with parameters defined in Table 5 for an arbitrary input signal with its set of dynamic phasors defined in Table 6. In this case, the choice of n_h was not as significant as the choice of N_{div} due to the large amplitude of the voltage unbalance during the time-interval $t \in (180, 480]$ ms, which is limited by the convergence of the inverse function Taylor series.

However, the time-interval $t \in (480, 800]$ ms demonstrates the need for a higher N_h as means of accurately expressing the d-axis components as well as the frequency estimation. Note that the amplitude of the distortions should be lower for an adequate choice of loop filter, which can lead to a lower number of components needed to accurately express these signals.

The number of terms of the rotation N_g was not significant since in this case the amplitude of the displacement angle dynamic phasor $\langle \delta \rangle_h, \forall h \neq 0$ is sufficiently small.

V. EXPERIMENTAL RESULTS

The Large Signal SRF-PLL model was employed together with a thorough HSS model of a grid-connected converter. The converter model is here suppressed, as it is the scope for future works. A state-feedback control with resonant controllers and a nonlinear state estimator was employed for the current control strategy, and a weak-grid with a Short Circuit Ratio (SCR) of approximately 1.5 for 10 kW/380 V base values, assuming 1 p.u. voltage. A 2DOF-PI controller was used for active power generation in a grid following control strategy. Results were obtained in the 8 kW range due to instabilities observed in the 10 kW range, resulting in a SCR of approximately 1.875. The control strategy was implemented in an FPGA-Microprocessor implementation, and the converter model was simulated via an OPAL-RT Hardware-in-the-loop due to the characteristic of the test conditions. The time constants were scaled by a factor of 100 to accurately represent the switched characteristic of power converter systems. Figure 9 depicts the converter model. The dc bus was composed by a constant current source and a dc bus capacitor.

Figure 10 demonstrates multiple unbalance steps, with a more detailed picture depicted by Figures 11 and 12. A minor deviation of $\langle \delta \rangle_0$ can be seen due to the losses caused by the switched characteristic of power converters, which in turn reduces the power injection, reducing the angle between grid and filter capacitor voltages, combined with modeling errors due to truncation, as discussed in the previous section. In this case, the PLL models had a total of three harmonic components $n_h = 3$, with the number of terms of the normalization $N_{div} = 2$ and the number of terms for the rotation $N_g = 2$. Small deviations in the dc bus voltage are caused by the truncation of the number of harmonics.

The model results enable a representation of the coupling between harmonics, as unbalanced voltages causes double harmonics in the PLL control loop, which are also fed back into the system. These results aim to demonstrate the accuracy of the PLL models for grid converter applications, which are suitable for further analysis.

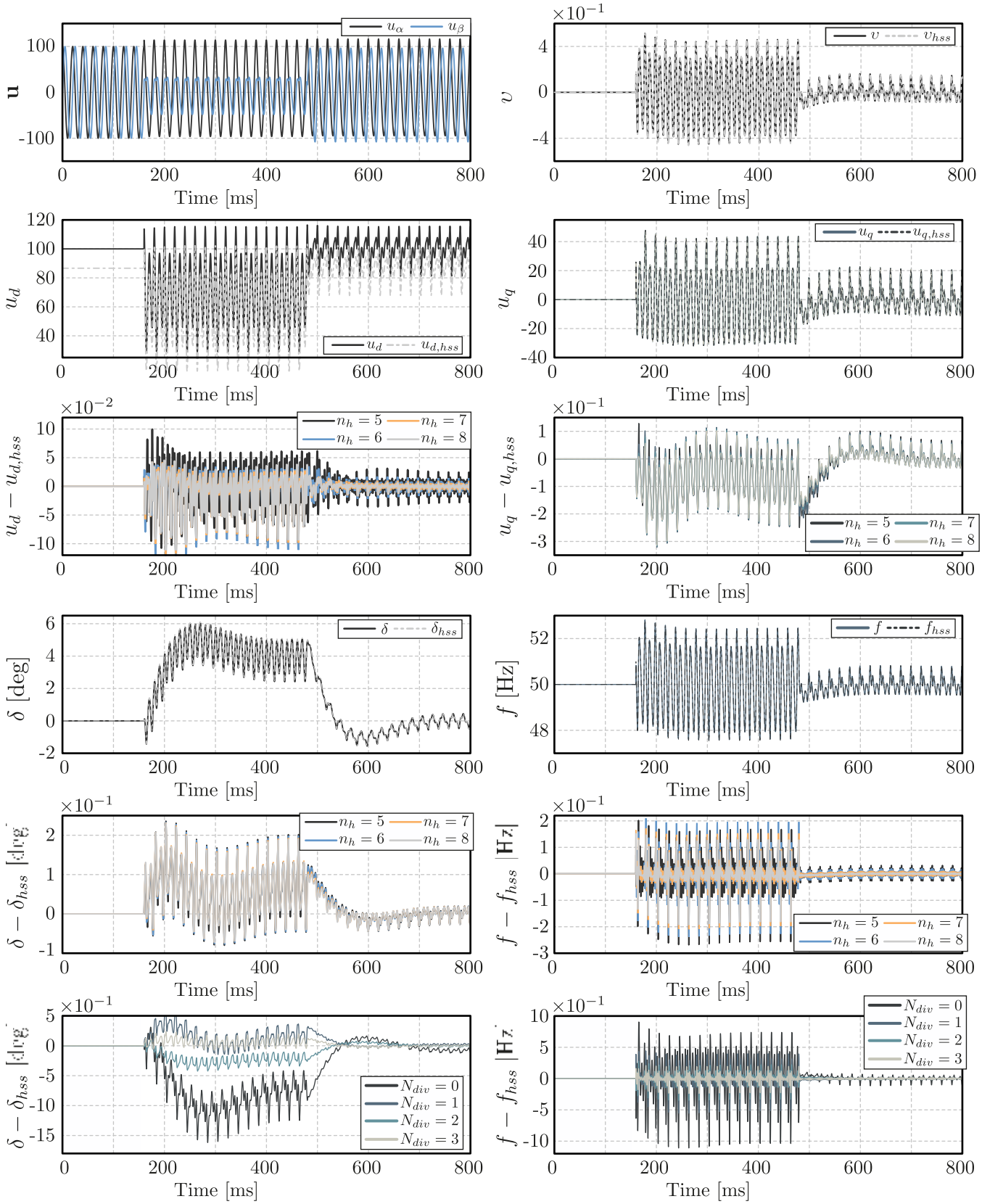

FIGURE 8. Validation of the proposed harmonic domain-based SRF-PLL model with a PI loop filter with gains given by Table 5 for an arbitrary input signal $\mathbf{u}$ with its phasors amplitudes and phases given by Table 6. The error is defined as the absolute error between the real valued function and the projection of the approximation onto the $L^2(\mathbb{R})$ space.

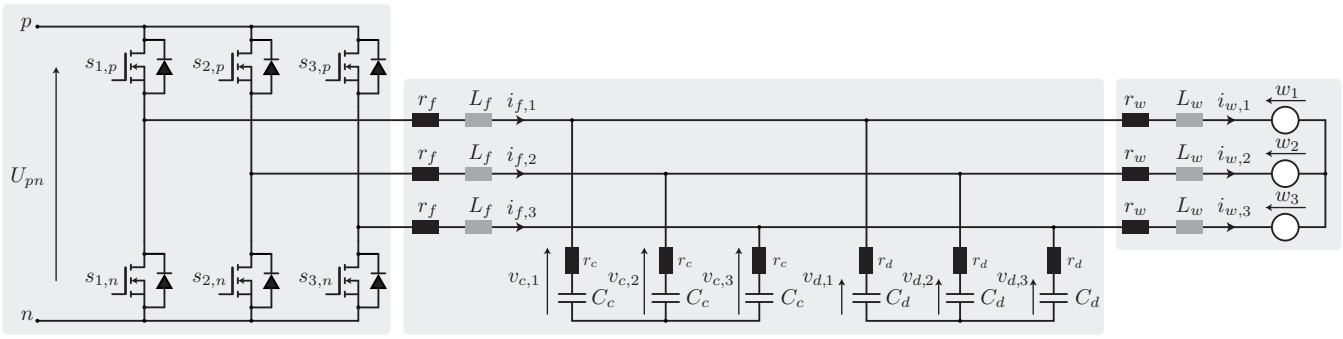

FIGURE 9. Converter model for experimental validation.

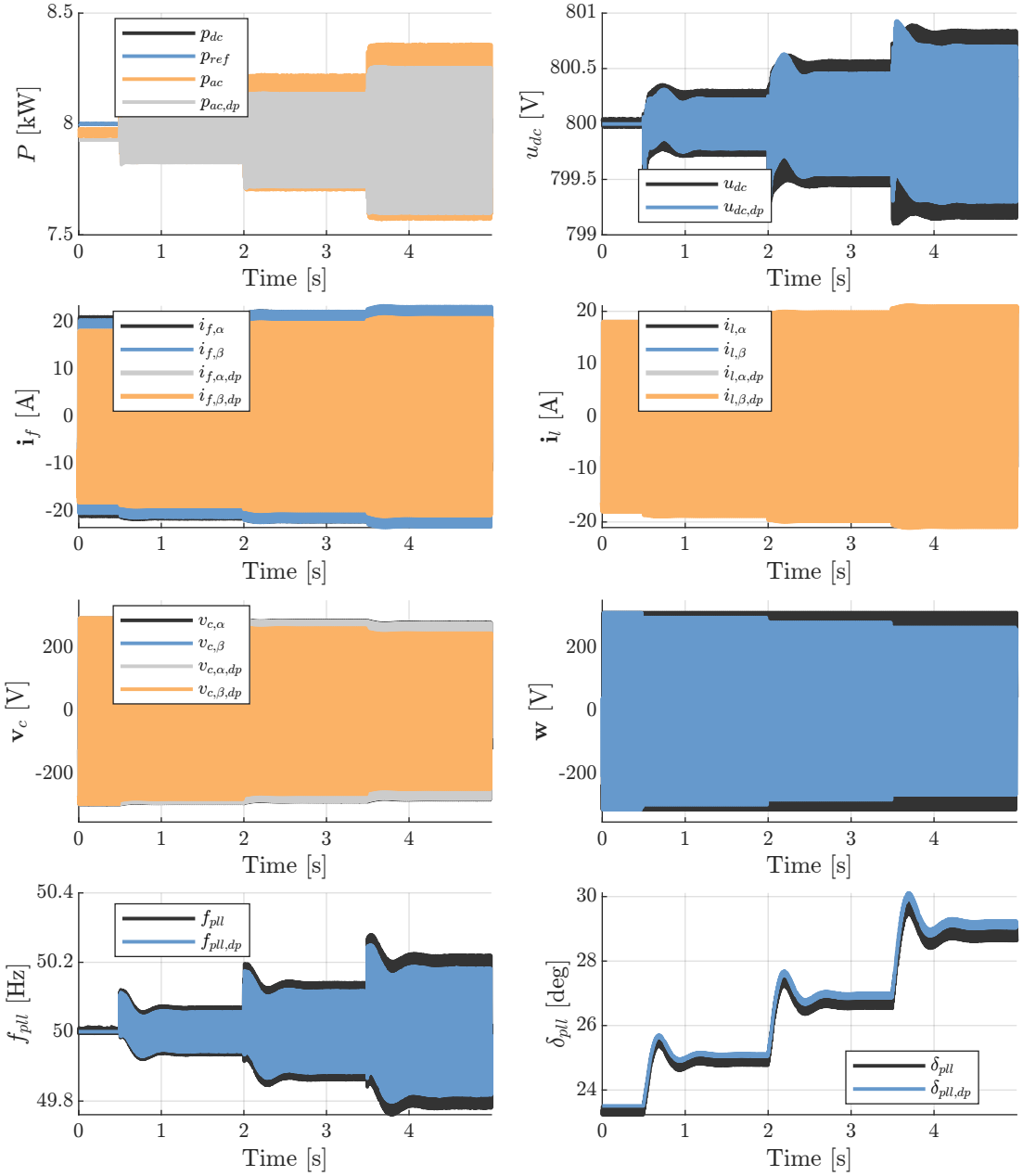

FIGURE 10. Mathematical model validation via hardware-in-the-loop for voltage unbalances, with β-axis voltage amplitude step from 1 p.u. to 0.85 p.u. in steps of 0.5 p.u. The subscript dp denotes the projection of the simulation values over the $L(\mathbb{R})$ space.

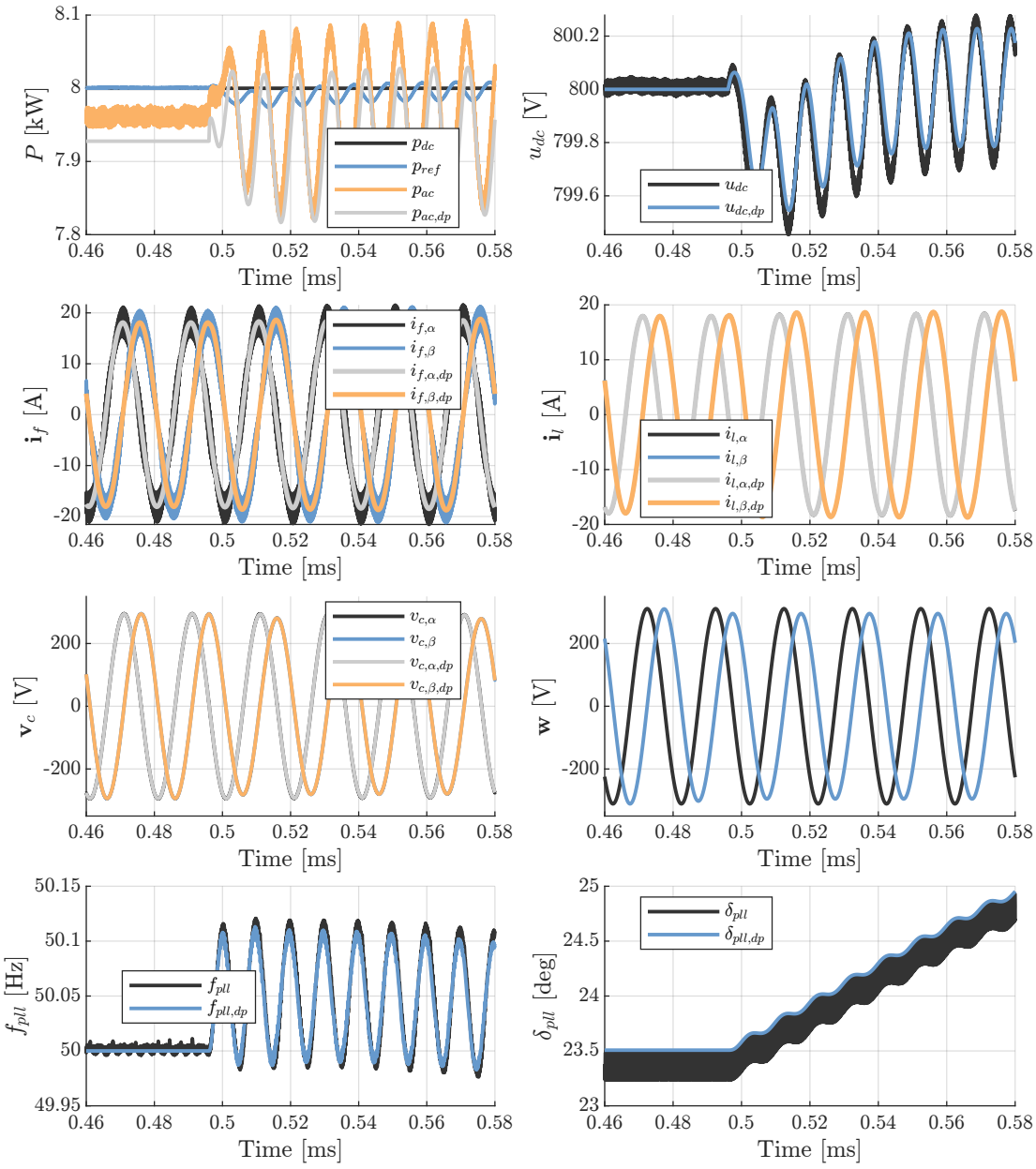

FIGURE 11. Mathematical model validation via hardware-in-the-loop for voltage unbalances, with β-axis voltage amplitude step from 1 p.u. to 0.95 p.u. The subscript dp denotes the projection of the simulation values over the $L(\mathbb{R})$ space.

VI. CONCLUSIONS

This work demonstrated a Harmonic State-Space modeling procedure for complex nonlinear functions as means of polynomial nonlinear systems with the objective of obtaining nonlinear large-signal models for the Park Transformation and the SRF-PLL. This was performed in terms of the dynamic phasors of an input in the $\alpha\beta$ coordinates and leads to fairly general models that can be used to address control analysis and synthesis for grid connected power electronic systems. These models are useful for different time-variant dynamical systems as means of obtaining a time-invariant description, which can be employed for obtaining equilibrium points. They are specially useful for studies on stability and bifurcation analysis.

An analysis of the dynamical system perturbations and responses is required to define the number of harmonics, as well as of the number of terms in the Taylor Series that employed for modeling the more complex functions. Once this is performed, the resulting analytical models also provide a straightforward and fast evaluation of the steady state performance of the system under study without requiring the execution of lengthy simulations. Thus, this enables the generation of automatic design tools that consider both controller tuning and the impact of varying physical parameters of the system.

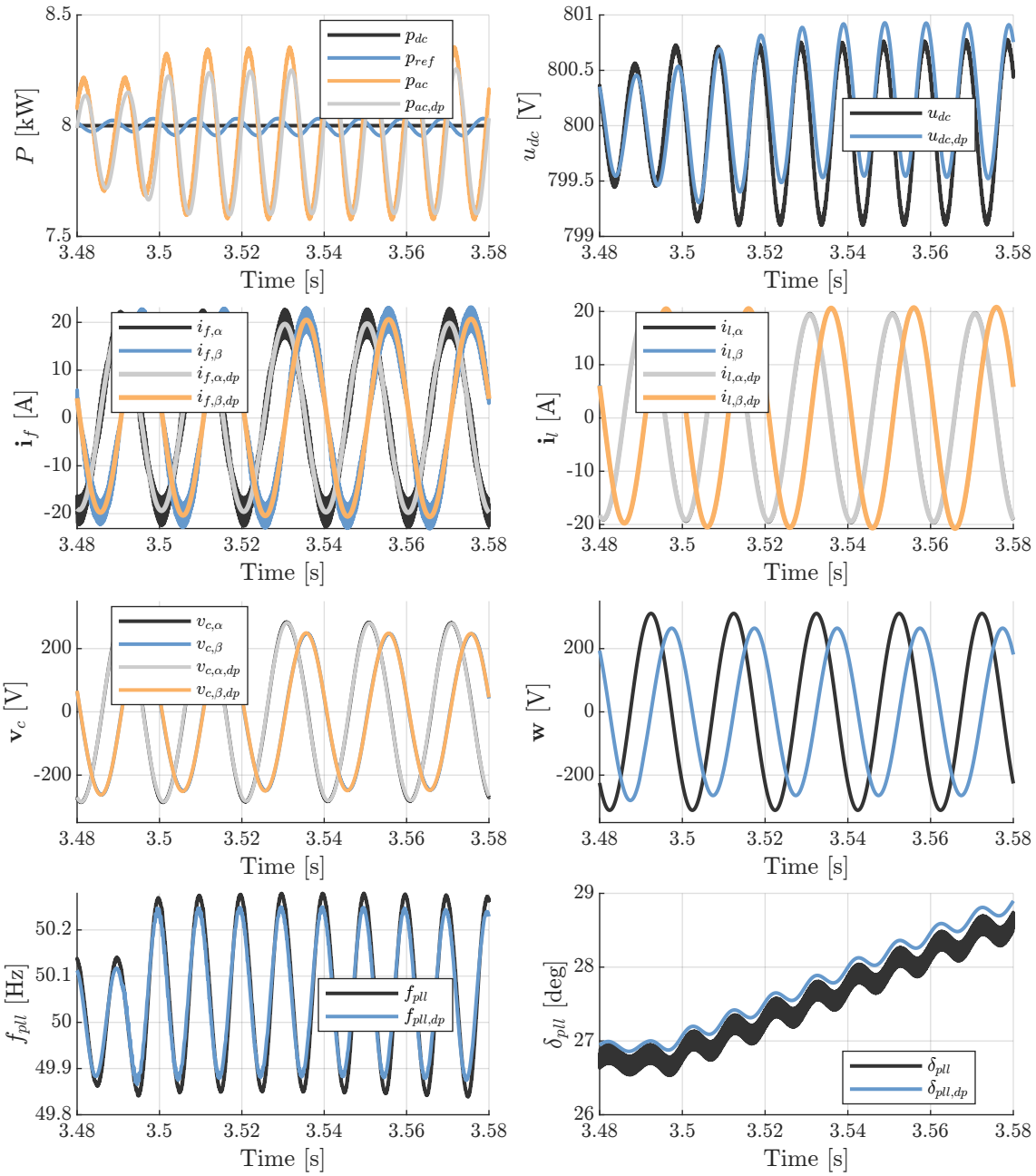

FIGURE 12. Mathematical model validation via hardware-in-the-loop for voltage unbalances, with β-axis voltage amplitude step from 0.9 p.u. to 0.85 p.u. The subscript dp denotes the projection of the simulation values over the $L(\mathbb{R})$ space.

AUTHOR'S CONTRIBUTIONS

GRABOVSKI, E.F.C.: Conceptualization, Data Curation, Formal Analysis, Investigation, Methodology, Software, Validation, Visualization, Writing – Original Draft, Writing – Review & Editing. **MUSSA, S.A.**: Conceptualization, Formal Analysis, Funding Acquisition, Investigation, Methodology, Resources, Supervision, Validation, Visualization, Writing – Review & Editing. **HELDWEIN, M.L.**: Conceptualization, Formal Analysis, Funding Acquisition, Investigation, Methodology, Resources, Supervision, Validation, Visualization, Writing – Original Draft, Writing – Review & Editing.

PLAGIARISM POLICY

This article was submitted to the similarity system provided by Crossref and powered by iThenticate – Similarity Check.

REFERENCES

[1] F. Blaabjerg, Y. Yang, D. Yang, X. Wang, "Distributed Power-Generation Systems and Protection", *Proceedings of the IEEE*, vol. 105, no. 7, pp. 1311–1331, 2017, doi:10.1109/JPROC.2017.2696878.

[2] X. Wang, F. Blaabjerg, "Harmonic Stability in Power Electronic-Based Power Systems: Concept, Modeling, and Analysis", *IEEE Transactions on Smart Grid*, vol. 10, no. 3, pp. 2858–2870, 2019, doi:10.1109/TSG.2018.2812712.

[3] D. E. Olivares, A. Mehrizi-Sani, A. H. Etemadi, C. A. Cañizares, R. Iravani, M. Kazerani, A. H. Hajimiragha, O. Gomis-Bellmunt, M. Saeedifard, R. Palma-Behnke, G. A. Jiménez-Estévez, N. D. Hatziargyriou, "Trends in Microgrid Control", *IEEE Transactions on Smart Grid*, vol. 5, no. 4, pp. 1905–1919, 2014, doi:10.1109/TSG.2013.2295514.

[4] J. M. Guerrero, M. Chandorkar, T.-L. Lee, P. C. Loh, "Advanced Control Architectures for Intelligent Microgrids—Part I: Decentralized and Hierarchical Control", *IEEE Transactions on Industrial Electronics*, vol. 60, no. 4, pp. 1254–1262, 2013, doi:10.1109/TIE.2012.2194969.

[5] B. M. Eid, N. A. Rahim, J. Selvaraj, A. H. El Khateb, "Control Methods and Objectives for Electronically Coupled Distributed Energy Resources in Microgrids: A Review", *IEEE Systems Journal*, vol. 10, no. 2, pp. 446–458, 2016, doi:10.1109/JSYST.2013.2296075.

[6] L. Harnefors, X. Wang, A. G. Yepes, F. Blaabjerg, "Passivity-Based Stability Assessment of Grid-Connected VSCs—An Overview", *IEEE Journal of Emerging and Selected Topics in Power Electronics*, vol. 4, no. 1, pp. 116–125, 2016, doi:10.1109/JESTPE.2015.2490549.

[7] E. Mollerstedt, B. Bernhardsson, "Out of control because of harmonics-an analysis of the harmonic response of an inverter locomotive", *IEEE Control Systems Magazine*, vol. 20, no. 4, pp. 70–81, 2000, doi:10.1109/37.856180.

[8] E. Lenz, D. J. Pagano, A. Ruseler, M. L. Heldwein, "Two-Parameter Stability Analysis of Resistive Droop Control Applied to Parallel-Connected Voltage-Source Inverters", *IEEE Journal of Emerging and Selected Topics in Power Electronics*, vol. 8, no. 4, pp. 3318–3332, 2020, doi:10.1109/JESTPE.2020.2971425.

[9] V. Caliskan, O. Verghese, A. Stankovic, "Multifrequency averaging of DC/DC converters", *IEEE Transactions on Power Electronics*, vol. 14, no. 1, pp. 124–133, 1999, doi:10.1109/63.737600.

[10] J. E. Ormrod, *Harmonic state space modelling of voltage source converters*, Master's thesis, University of Canterbury, 2013.

[11] F. Blaabjerg, R. Teodorescu, M. Liserre, A. Timbus, "Overview of Control and Grid Synchronization for Distributed Power Generation Systems", *IEEE Transactions on Industrial Electronics*, vol. 53, no. 5, pp. 1398–1409, 2006, doi:10.1109/TIE.2006.881997.

[12] J. B. Kwon, X. Wang, F. Blaabjerg, C. L. Bak, A. R. Wood, N. R. Watson, "Harmonic Instability Analysis of a Single-Phase Grid-Connected Converter Using a Harmonic State-Space Modeling Method", *IEEE Transactions on Industry Applications*, vol. 52, no. 5, pp. 4188–4200, 2016, doi:10.1109/TIA.2016.2581154.

[13] J. Z. Zhou, H. Ding, S. Fan, Y. Zhang, A. M. Gole, "Impact of Short-Circuit Ratio and Phase-Locked-Loop Parameters on the Small-Signal Behavior of a VSC-HVDC Converter", *IEEE Transactions on Power Delivery*, vol. 29, no. 5, pp. 2287–2296, 2014, doi:10.1109/TPWRD.2014.2330518.

[14] X. Wang, L. Harnefors, F. Blaabjerg, "Unified Impedance Model of Grid-Connected Voltage-Source Converters", *IEEE Transactions on Power Electronics*, vol. 33, no. 2, pp. 1775–1787, 2018, doi:10.1109/TPEL.2017.2684906.

[15] D. Dong, B. Wen, D. Boroyevich, P. Mattavelli, Y. Xue, "Analysis of Phase-Locked Loop Low-Frequency Stability in Three-Phase Grid-Connected Power Converters Considering Impedance Interactions", *IEEE Transactions on Industrial Electronics*, vol. 62, no. 1, pp. 310–321, 2015, doi:10.1109/TIE.2014.2334665.

[16] G. Gao, X. Wang, T. Zhu, Y. Liao, J. Tong, "HSS Modeling and Stability Analysis of Single-Phase PFC Converters", *in 2022 IEEE Applied Power Electronics Conference and Exposition (APEC)*, pp. 1812–1819, 2022, doi:10.1109/APEC43599.2022.9773776.

[17] P. Rodriguez, J. Pou, J. Bergas, I. Candela, R. Burgos, D. Boroyevich, "Double Synchronous Reference Frame PLL for Power Converters Control", *in 2005 IEEE 36th Power Electronics Specialists Conference*, pp. 1415–1421, 2005, doi:10.1109/PESC.2005.1581815.

[18] B. Liu, F. Zhuo, Y. Zhu, H. Yi, F. Wang, "A Three-Phase PLL Algorithm Based on Signal Reforming Under Distorted Grid Conditions", *IEEE Transactions on Power Electronics*, vol. 30, no. 9, pp. 5272–5283, 2015, doi:10.1109/TPEL.2014.2366104.

[19] S. Golestan, J. M. Guerrero, J. C. Vasquez, "Three-Phase PLLs: A Review of Recent Advances", *IEEE Transactions on Power Electronics*, vol. 32, no. 3, pp. 1894–1907, 2017, doi:10.1109/TPEL.2016.2565642.

[20] J. B. Kwon, X. Wang, F. Blaabjerg, C. L. Bak, "Precise model analysis for 3-phase high power converter using the Harmonic State Space modeling", *in 2015 9th International Conference on Power Electronics and ECCE Asia (ICPE-ECCE Asia)*, pp. 2628–2635, 2015, doi:10.1109/ICPE.2015.7168177.

[21] J. Kwon, X. Wang, C. L. Bak, F. Blaabjerg, "Harmonic instability analysis of single-phase grid connected converter using Harmonic State Space (HSS) modeling method", *in 2015 IEEE Energy Conversion Congress and Exposition (ECCE)*, pp. 2421–2428, 2015, doi:10.1109/ECCE.2015.7310001.

[22] Y. Liao, X. Wang, "Small-Signal Modeling of AC Power Electronic Systems: Critical Review and Unified Modeling", *IEEE Open Journal of Power Electronics*, pp. 1–1, 2021, doi:10.1109/OJPEL.2021.3104522.

BIOGRAPHIES

Edhuardo Francisco Celli Grabovski received the B.S. and M.S. degrees in electrical engineering from the Federal University of Santa Catarina (UFSC), Florianopolis, Brazil, in 2016 and 2018, respectively, currently working towards the Ph.D. degree in electrical engineering from INEP–UFSC. He is currently a Senior Power Electronics Engineer, consultant for Huawei Technologies Sweden, AB, Stockholm, Sweden. His research interests include power electronics, modeling, control and stability analysis of power converter systems and optimal design of power converters.

Samir Ahmad Mussa received the B.S. degree from the Federal University of Santa Maria (UFSM) in 1988, and the M.S. and Ph.D. degrees from the Federal University of Santa Catarina (UFSC), in 1994 and 2003, respectively. He is currently a Full Professor at the Electrical and Electronics Engineering Department (EEL) of the Federal University of Santa Catarina (UFSC) and researcher at the Power Electronics Institute (INEP). His research interests include PFC rectifiers, Digital Signal Processing, DSP, FPGA and microprocessor-based systems. Dr. Mussa is a member of the Brazilian Power Electronic Society (SOBRAEP) and IEEE.

Marcelo Lobo Heldwein received the B.S. and M.S. degrees in electrical engineering from the Federal University of Santa Catarina (UFSC), Florianópolis, Brazil, in 1997 and 1999, respectively, and the Ph.D. degree from the Swiss Federal Institute of Technology (ETH Zürich), in 2007. From 1999 to 2003, he worked with industry, including research and development activities at the Power Electronics Institute, Brazil and Emerson Network Power, Brazil and Sweden. He was a Postdoctoral Fellow at the ETH Zürich and at the UFSC, from 2007 to 2009. From 2010 to 2022, he was a Professor with the Department of Electronics and Electrical Engineering, UFSC. He is currently the Head of the Chair of High–Power Converter Systems (HLU), at the Technical University of Munich (TUM). His research interests include power electronics, advanced power distribution technologies, and electromagnetic compatibility. He is a member of the Brazilian Power Electronic Society (SOBRAEP), a Senior member of the IEEE and a member of the Advisory Board of PCIM Europe.